The Face of Art: Landmark Detection and Geometric Style in Portraits - Supplemental material

JORDAN YANIV, Tel Aviv University & The Interdisciplinary Center, Herzliya
YAEL NEWMAN, Tel Aviv University & The Interdisciplinary Center, Herzliya
ARIEL SHAMIR, The Interdisciplinary Center, Herzliya

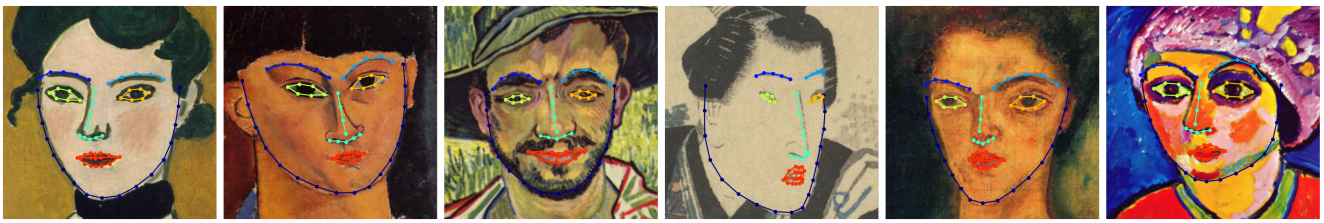

Fig. 1. More landmark detection results on different artistic portrait styles using our proposed method for Artistic Facial Feature Detection.
From left to right: Marguerite, 1907 by Henri Matisse courtesy WikiArt [Public Domain US] via (https://www.wikiart.org/en/henri-matisse/marguerite-1907), Portrait of Moise Kisling, 1916 by Amedeo Modigliani courtesy WikiArt [Public Domain] via (https://www.wikiart.org/en/amedeo-modigliani/portrait-of-moise-kisling-1916), Portrait of a Young Peasant, 1889 by Vincent van Gogh courtesy WikiArt [Public Domain] via (https://www.wikiart.org/en/vincent-van-gogh/portrait-of-a-young-peasant-1889), Actor and Woman on a Riverbank, 1820-1830 by Utagawa Kunisada courtesy Van Gogh Museum [Public Domain] via (https://www.vangoghmuseum.nl/en/japanese-prints/collection/n0140V1962), Martha Hirsch, 1909 by Oskar Kokoschka courtesy WikiArt [Public Domain US] via (https://www.wikiart.org/en/oskar-kokoschka/not_detected_235850), Der violette Turban, 1911 by Alexej von Jawlensky courtesy WikiArt [Public Domain] via (https://www.wikiart.org/en/alexej-von-jawlensky/der-violette-turban-1911).

CCS Concepts: • **Computing methodologies** → *Image processing*; Image representations; *Non-photorealistic rendering*; *Neural networks*.

Additional Key Words and Phrases: facial landmark detection , neural networks, artistic image augmentation, geometry aware style transfer

1 IMPLEMENTATION DETAILS

In this section we report the parameter values used in our implementation and training procedure.

Network Architecture. The network consists of three connected subnetworks, namely the PrimaryNet, FusionNet and UpsampleNet. Given an input image with the size of 256×256, the first two subnetworks regress smaller heatmaps with the size of 64×64. The last UpsampleNet is simply a deconvolutional layer which bilinearly upsamples the feature maps back to the size of the input image.

The STN subnetwork architecture used to predict the transformation parameters. The transformation is applied on a grid and sampled with bilinear interpolation. We applied the STN directly on the heat-maps before upsampling (see Tables 1 and 2 for architecture details).

Texture Style Augmentation Parameters. For the texture augmentation process, we follow the texture modelling approach proposed by Gatys et al. [2015] and use the Gram Matrix of the VGG16 feature maps [Simonyan and Zisserman 2015].

Given a content image $\mathcal{I}_c$ and a style image $\mathcal{I}_s$, the algorithm tries to seek a stylised image $\mathcal{I}$ that minimises the following objective:

$$\mathcal{I}^* = \arg\min_{\mathcal{I}} \alpha \mathcal{L}_c(\mathcal{I}_c, \mathcal{I}) + \beta \mathcal{L}_s(\mathcal{I}_s, \mathcal{I})$$

where $\mathcal{L}_c$ compares the content representation of a given content image to that of the stylised image, and $\mathcal{L}_s$ compares the Gram-based style representation derived from a style image to that of the stylised image. α and β are used to balance the content component and style component in the stylised result. The loss is minimized using ADAM optimizer [2015] for 100 iterations.

We use the following parameters to perform texture style transfer in our augmentation pipeline:

- $\alpha = 1$ (content weight)
- $\beta = 1000$ (style weight)
- VGG layers for style loss: conv_1_2, conv_2_2, conv_3_3, conv_4_3, conv_5_3
- VGG layers for content loss: conv_4_3, conv_5_3
- Style image is resized to 256×256

Geometric Style Augmentation Parameters. Geometric augmentation is applied by randomly distorting the input pair $(\mathcal{I}, \mathbf{l}^*)$ of face image $\mathcal{I}$ and ground truth landmarks $\mathbf{l}^*$. The landmarks of each facial feature f are transformed accordingly:

$$\mathbf{l}'_f = F(\mathbf{l}^*_f; s_{x_f}, s_{y_f}, t_{x_f}, t_{y_f})$$

where $\mathbf{l}^*_f$ is a subset of the ground truth landmarks, belonging to a certain facial feature f, s_{x_f}, s_{y_f} and t_{x_f}, t_{y_f} are the scaling and translation factors for the x and y coordinates of feature f respectively. The scaling and translation factors are sampled from a uniform distribution with given lower and upper bounds for each transformation parameter. Scaling bounds are fixed, and translation bounds are calculated using input face geometry. These parameters were chosen to enable maximum variation in the facial feature locations and size, without causing artifacts. Lower and upper bounds of

Authors' addresses: Jordan Yaniv, Tel Aviv University & The Interdisciplinary Center, Herzliya, jordanya@mail.tau.ac.il; Yael Newman, Tel Aviv University & The Interdisciplinary Center, Herzliya, yaelnewman@mail.tau.ac.il; Ariel Shamir, The Interdisciplinary Center, Herzliya, arik@idc.ac.il.

Table 1. Network Architecture

Sub-Network	Name	Shape-in	Shape-out	Kernel	ReLU	Pool
Primary	conv_1	256x256x3	128x128x128	5x5x128, 1, 1	TRUE	TRUE
Primary	conv_2	128x128x128	64x64x128	5x5x128, 1, 1	TRUE	TRUE
Primary	conv_3	64x64x128	64x64x128	5x5x128, 1, 1	TRUE	FALSE
Primary	conv_4_1	64x64x128	64x64x128	3x3x128, 1, 1	TRUE	FALSE
Primary	conv_4_2	64x64x128	64x64x128	3x3x128, 1, 2	TRUE	FALSE
Primary	conv_4_3	64x64x128	64x64x128	3x3x128, 1, 3	TRUE	FALSE
Primary	conv_4_4	64x64x128	64x64x128	3x3x128, 1, 4	TRUE	FALSE
Primary	concat_4	-	64x64x512	-	-	-
Primary	conv_5_1	64x64x512	64x64x256	3x3x256, 1, 1	TRUE	FALSE
Primary	conv_5_2	64x64x512	64x64x256	3x3x256, 1, 2	TRUE	FALSE
Primary	conv_5_3	64x64x512	64x64x256	3x3x256, 1, 3	TRUE	FALSE
Primary	conv_5_4	64x64x512	64x64x256	3x3x256, 1, 4	TRUE	FALSE
Primary	concat_5	-	64x64x1024	-	-	-
Primary	conv_6	64x64x1024	64x64x512	1x1x512, 1, 1	TRUE	FALSE
Primary	conv_7	64x64x512	64x64x256	1x1x256, 1, 1	TRUE	FALSE
Primary	primary_out	64x64x256	64x64x68	1x1x68, 1, 1	FALSE	FALSE
Fusion	concat_0	-	64x64x384	-	-	-
Fusion	conv_1_1	64x64x384	64x64x64	3x3x64, 1, 1	TRUE	FALSE
Fusion	conv_1_2	64x64x384	64x64x64	3x3x64, 1, 2	TRUE	FALSE
Fusion	conv_1_3	64x64x384	64x64x64	3x3x64, 1, 3	TRUE	FALSE
Fusion	concat_1	-	64x64x192	-	-	-
Fusion	conv_2_1	64x64x192	64x64x64	3x3x64, 1, 1	TRUE	FALSE
Fusion	conv_2_2	64x64x192	64x64x64	3x3x64, 1, 2	TRUE	FALSE
Fusion	conv_2_3	64x64x192	64x64x64	5x5x64, 1, 3	TRUE	FALSE
Fusion	conv_2_4	64x64x192	64x64x64	3x3x64, 1, 4	TRUE	FALSE
Fusion	concat_2	-	64x64x256	-	-	-
Fusion	conv3_1	64x64x256	64x64x128	3x3x128, 1, 1	TRUE	FALSE
Fusion	conv3_2	64x64x256	64x64x128	3x3x128, 1, 2	TRUE	FALSE
Fusion	conv3_3	64x64x256	64x64x128	5x5x128, 1, 3	TRUE	FALSE
Fusion	conv3_4	64x64x256	64x64x128	3x3x128, 1, 4	TRUE	FALSE
Fusion	concat_3	-	64x64x512	-	-	-
Fusion	conv4	64x64x512	64x64x256	1x1x256, 1, 1	TRUE	FALSE
Fusion	fusion_out	64x64x256	64x64x68	1x1x68, 1, 1	FALSE	FALSE
STN	stn_out	64x64x68	64x64x68	-	-	-
Upsample	out	64x64x68	256x256x68	8x8x68, 4, 1	FALSE	FALSE

Note: The filter parameter of each layer is denoted in the form of (kernel width x kernel height x number of channels, stride , dilation), where dilation=1 means that there is no dilation. concat_i layers refers to the concatenation of conv_i_j layers. The only exception is concat_0 layer (in Fusion sub-network), which concatenates the layers conv_3 & conv_7 of the Primary sub-network.

Table 2. STN Architecture

Name	Shape-in	Shape-out	Kernel	ReLU	Pool
conv_1	64x64x68	32x32x64	3x3x64, 1, 1	TRUE	TRUE
conv_2	32x32x64	16x16x32	3x3x32, 1, 1	TRUE	TRUE
out	16x16x32	6	-	FALSE	-

The STN subnetwork architecture used to predict the transformation parameters. The third layer is a fully-connected layer that outputs 6 parameters for an affine transformation.

Table 3. Scaling parameters for Geometric Style Augmentation

Feature	x		y	
	l_b	u_b	l_b	u_b
left eye + eyebrow	0.8	1.5	0.8	1.5
right eye + eyebrow	0.8	1.5	0.8	1.5
mouth	0.7	1.2	0.7	1.2
nose	0.7	1.5	0.7	1.0
jaw	0.6	1.2	0.6	1.2

Note: l_b and u_b refer to lower and upper bounds, respectively.

Table 4. number of PCs for feature based PDM

Feature	#PCs
left eyebrow	2
right eyebrow	2
left eye	3
right eye	3
mouth	7
nose	5
jaw	7

s_{x_f}, s_{y_f} are listed in Table 3, Lower and upper bounds of t_{x_f}, t_{y_f} are listed in Table 5.

Feature-based Correction Parameters. We create a separate PDM model for each facial feature, and at inference time, landmark subsets belonging to different facial features are fitted independently. The PDM models were trained on the natural faces training set [Sagonas et al. 2013], without any augmentations. In Table 4, we report the number of Principal Components (PCs) used to create the PDM model of each facial feature. These numbers were optimized using the full-A set.

2 ADDITIONAL EVALUATION

In this section we provide additional evaluation of our method. In Table 7 we compare our approach with recently proposed state of-the-art algorithms ([Lv et al. 2017], [Xiao et al. 2017], [Jourabloo et al. 2017]) on natural face images. Our method ($\mathbf{EC_pT_p + A}$) achieves results that are comparable with recent state-of-the-art methods. This implies that adding artistic augmentation to the training procedure, and a part-based correction for inference, enables using the same framework for detecting facial landmarks on both natural and artistic faces, and can be used as a detection component in cross-domain applications. We show the performance of different facial landmark detection algorithms on real artistic portraits in Table 6 using AUC and failure rate evaluation metrics. We use 3 different normalization methods for comparison; inter-ocular distance, inter-pupil distance and the diagonal of the ground truth bounding-box. Our method outperforms state-of-the-art methods that were trained on natural face data. Note that artistic augmentation can be added to the training procedure of any algorithm to enhance performance on artistic portraits.

3 APPLICATIONS

Our framework for facial landmark detection in art, allows both the analysis and synthesis of artistic portraits. In this section, we present additional results of potential applications that can make use of our framework.

Geometry-Aware Style Transfer. Figure 3 shows Geometry Aware Style Transfer examples. Our geometric stylization method can be combined with any texture style transfer method, to enhance stylization results. Figure 4 shows the effect of adding geometric stylization to different style transfer methods.

Artist's Geometric Style. Utilizing our proposed method for landmark detection in art, we can visualize the distribution of facial landmarks of a specific artist. As illustrated in Figure 5, such visualizations can highlight the differences in the geometric style of different artists. Observing these distributions, we can identify the style of artists: an elongated face and nose for Modigliani, a small face with large eyes for Keane, etc.

Style Signatures. We define a vector of 99 dimensions as the *geometric* style signature of a portrait. This signature vector includes the following set of values. Feature aspect-ratios are computed as $f_H : f_W$, for any facial feature f, where f_H and f_W represent the height and width of the feature's bounding box. For all pairs of features f^1, f^2, the relative proportion are computed as $f^1_H : f^2_H$, $f^1_W : f^2_W$ and $f^1_H : f^2_W$. The relative location of all inner facial features (mouth, eyes and eyebrows) are calculated as the normalized difference between the feature center point $\bar{f}$ and the face center point O in both directions: $FW^{-1}\left|\bar{f}_x - O_x\right|$, $FH^{-1}\left|\bar{f}_y - O_y\right|$, where $FW = \max(\mathbf{l}_x) - \min(\mathbf{l}_x)$ and $FH = \max(\mathbf{l}_y) - \min(\mathbf{l}_y)$. Other values included in the geometric style signature are facial proportions that have been reported to have correlation with beauty and attractiveness. In Table 8 we report a subset of facial Golden Ratios [Schmid et al. 2008] used in the style signature. In Table 9 we report a subset of Neoclassical Canons ratios [Farkas et al. 1985] used in the style signature. In Figures 6 we compare the embedding of the signatures of various artworks using texture only vs. our texture and geometry method. Adding geometric information to the texture style embedding results in a more holistic representation of the artworks, and allows better examination of artist style similarities based on not just on textural and appearance attributes but also on the geometrical style.

4 ARTISTIC-FACES DATASET

The Artistic-Faces dataset contains 160 artistic portraits. To keep consistent with previous works in facial landmark detection of natural faces, the portraits are annotated with 68 facial landmarks. The dataset consists of artworks of 16 different artists, which were chosen to be representative of a wide range of artistic styles, both in geometry and texture. Figures 7 and 8 shows example artworks (that are not copyright, or we attained permission) out of the Artistic-Faces dataset.

Table 5. Translation parameters for Geometric Style Augmentation

Feature	l_b
left eye + eyebrow	x_0 + 0.5·(min(left eye ∪ eyebrow) - x_0)
right eye + eyebrow	max(upper nose) + 0.5·(min(right eye ∪ eyebrow) - max(upper nose))
mouth	min (lower jaw) - 0.5·(min(mouth) - min(lower jaw))
nose	max(left eye) + 0.5·(min(upper nose) - max(left eye))

(a) x translation lower bound

Feature	u_b
left eye + eyebrow	max(left eye ∪ eyebrow) +0.5·(min(upper nose)-max(left eye ∪ eyebrow))
right eye + eyebrow	max(right eye ∪ eyebrow) +0.5·(x_{16} - max(right eye ∪ eyebrow))
mouth	max(mouth) +0.5·(max(lower jaw) - max(mouth))
nose	max(nose1) + 0.5·(min(right eye) - max(upper nose))

(b) x translation upper bound

Feature	l_b
left eye + eyebrow	0
right eye + eyebrow	0
mouth	max(nose) + 0.5·(min(mouth) - max(nose))
nose	min(nose) + 0.5·(max(eye brows) - min(nose))

(c) y translation lower bound

Feature	u_b
left eye + eyebrow	max(left eye) + 0.25·(y_{33} - max(left eye))
right eye + eyebrow	max(right eye ∪ eyebrow) + 0.25·(y_{33} - max(right eye ∪ eyebrow))
mouth	max(jaw) - 0.5·(max(jaw) - max(mouth))
nose	max(nose)

(d) y translation upper bound

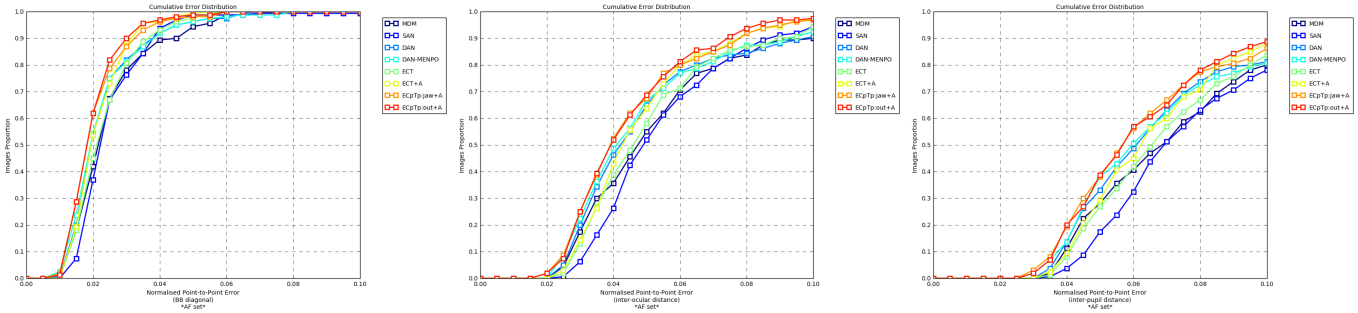

(a) normalized by BB diagonal (b) normalized by inter-ocular distance (c) normalized by inter-pupil distance

Fig. 2. Comparison of cumulative errors distribution (CED) curves on the Artistic-Faces dataset

REFERENCES

X. Cao, Y. Wei, F. Wen, and J. Sun. 2014. Face Alignment by Explicit Shape Regression. *Proceedings of the International Journal of Computer Vision (IJCV)* 107, 2 (2014), 177–190.

X. Dong, Y. Yan, W. Ouyang, and Y. Yang. 2018. Style Aggregated Network for Facial Landmark Detection. In *Proceedings of the IEEE Conference on Computer Vision and Pattern Recognition (CVPR)*. 379–388.

L.-G. Farkas, T.-A. Hreczko, J.-C. Kolar, and I.-R. Munro. 1985. Vertical and Horizontal Proportions of the Face in Young Adult North American Caucasians: Revision of Neoclassical Canons. *Plastic and Reconstructive Surgery (PRS)* 75, 3 (1985), 328âĂŞ337.

L.-A. Gatys, A.-S. Ecker, and M. Bethge. 2015. A Neural Algorithm of Artistic Style. (2015). arXiv:arXiv:1508.06576

X. Huang and S.-J. Belongie. 2017. Arbitrary Style Transfer in Real-Time with Adaptive Instance Normalization. *2017 IEEE International Conference on Computer Vision (ICCV)* (2017), 1510–1519.

Amin Jourabloo, Mao Ye, Xiaoming Liu, and Liu Ren. 2017. Pose-Invariant Face Alignment with a Single CNN. *2017 IEEE International Conference on Computer Vision (ICCV)* (2017), 3219–3228.

Diederik P. Kingma and Jimmy Ba. 2015. Adam: A Method for Stochastic Optimization. *CoRR* abs/1412.6980 (2015).

M. Kowalski, J. Naruniec, and T. Trzcinski. 2017. Deep Alignment Network: A Convolutional Neural Network for Robust Face Alignment. In *Proceedings of the IEEE Conference on Computer Vision and Pattern Recognition (CVPR)*. 2034–2043.

Y. Li, C. Fang, J. Yang, Z. Wang, X. Lu, and M.-H. Yang. 2017. Universal Style Transfer via Feature Transforms. In *NIPS*.

Fig. 3. Geometry + Texture Style Transfer examples. We can identify the signature geometric style of each artist; a small face with large eyes for Keane, a wide chin and large distance between the eyes for Leger, an elongated face and nose for Modigliani, distorted spatial locations of the different facial features for Picasso. Notice the second to last image, we can identify the signature Picasso style of integrating a profile into a frontal face drawing. In the last row, notice the signature style of Foujita; round, child-like face, with pointy chin, small mouth and large distance between the eyes. By combining both textural and geometrical elements for modelling artistic style, we achieve image stylization which is more visually appealing, maintains higher artistic credibility and present higher variation between images stylized using different artistic models. 1st row from [Minear and Park 2004], used with permission.

.

Table 6. Comparisons of AUC @ 0.08 (%) and Failure Rate (%) on the Artistic-Faces dataset (AF). Last two rows are our method.

	inter-pupil		inter-ocular		BB diagonl
Method	AUC	FR	AUC	FR	AUC
MDM	20.54	37.50	37.45	16.25	69.16
SAN	16.88	36.88	34.61	13.75	69.09
DAN	24.50	26.25	41.45	15.62	71.58
DAN-MENPO	25.57	27.50	42.06	12.50	71.92
ECT	20.63	33.13	38.49	13.12	71.03
ECT+A	22.88	29.37	41.45	8.13	73.25
$\mathbf{EC_pT_{p:jaw}+A}$	**27.63**	22.50	44.72	8.13	74.46
$\mathbf{EC_pT_{p:out}+A}$	27.32	**21.88**	**45.12**	**6.25**	**74.88**

J. Lv, X. Shao, J. Xing, C. Cheng, and X. Zhou. 2017. A Deep Regression Architecture with Two-Stage Re-initialization for High Performance Facial Landmark Detection. In *Proceedings of the IEEE Conference on Computer Vision and Pattern Recognition (CVPR)*. 3691–3700.

M. Minear and D. Park. 2004. A Lifespan Database of Adult Facial Stimuli. *Behavior research methods, instruments, & computers : a journal of the Psychonomic Society, Inc* 36 (12 2004), 630–3.

S. Ren, X. Cao, Y. Wei, and J. Sun. 2016. Face Alignment via Regressing Local Binary Features. *IEEE Transactions on Image Processing* 25, 3 (March 2016), 1233–1245.

C. Sagonas, G. Tzimiropoulos, S. Zafeiriou, and M. Pantic. 2013. 300 Faces in-the-Wild Challenge: The first facial landmark localization Challenge. In *Proceedings of the IEEE International Conference on Computer Vision (ICCV)*. 397–403.

K. Schmid, D. Marx, and A. Samal. 2008. Computation of face attractiveness index based on neoclassic canons, symmetry and golden ratio. *Pattern Recognition* 41, 8 (2008), 2710–2717.

K. Simonyan and A. Zisserman. 2015. Very Deep Convolutional Networks for Large-Scale Image Recognition. (2015), 14 pages.

G. Trigeorgis, P. Snape, M. Nicolaou, E. Antonakos, and S. Zafeiriou. 2016. Mnemonic Descent Method: A Recurrent Process Applied for End-to-End Face Alignment. *2016 IEEE Conference on Computer Vision and Pattern Recognition (CVPR)*, 4177–4187.

S. Xiao, J. Feng, L. Liu, X. Nie, W. Wang, S. Yan, and A. Kassim. 2017. Recurrent 3D-2D Dual Learning for Large-Pose Facial Landmark Detection. In *2017 IEEE International Conference on Computer Vision (ICCV)*. 1642–1651.

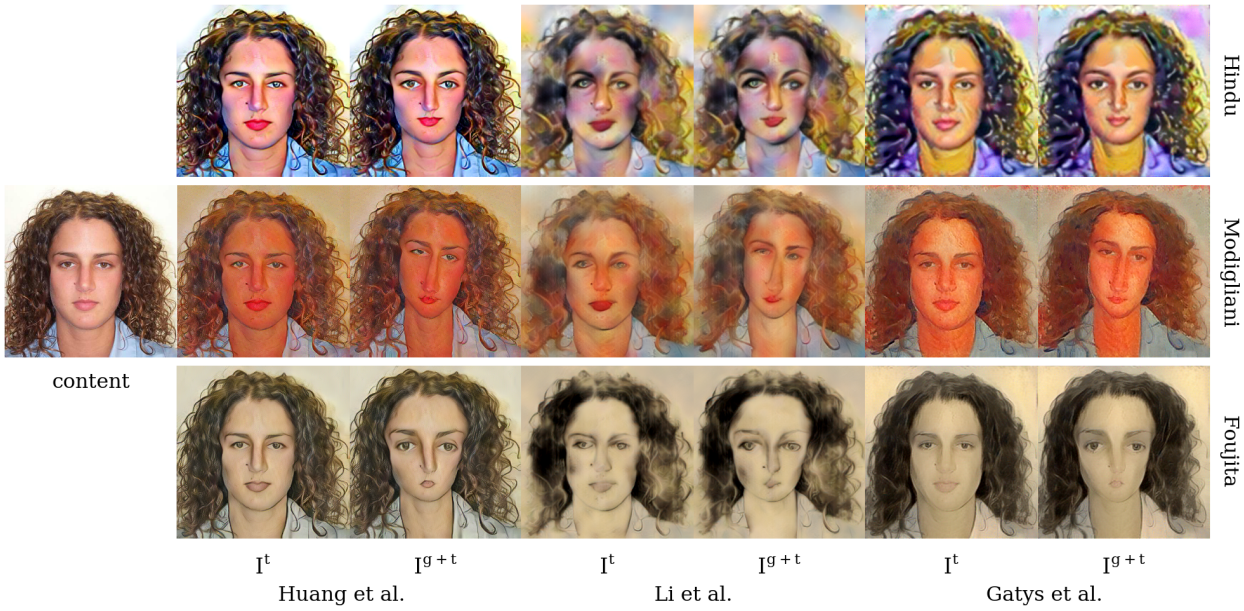

Fig. 4. Combining geometric stylization with different style transfer methods. Our geometric stylization method can be combined with any texture style transfer method, to enhance stylization results. For this comparison we used the style transfer methods proposed by Huang et al. [2017], Li et al. [2017] and Gatys et al. [2015].

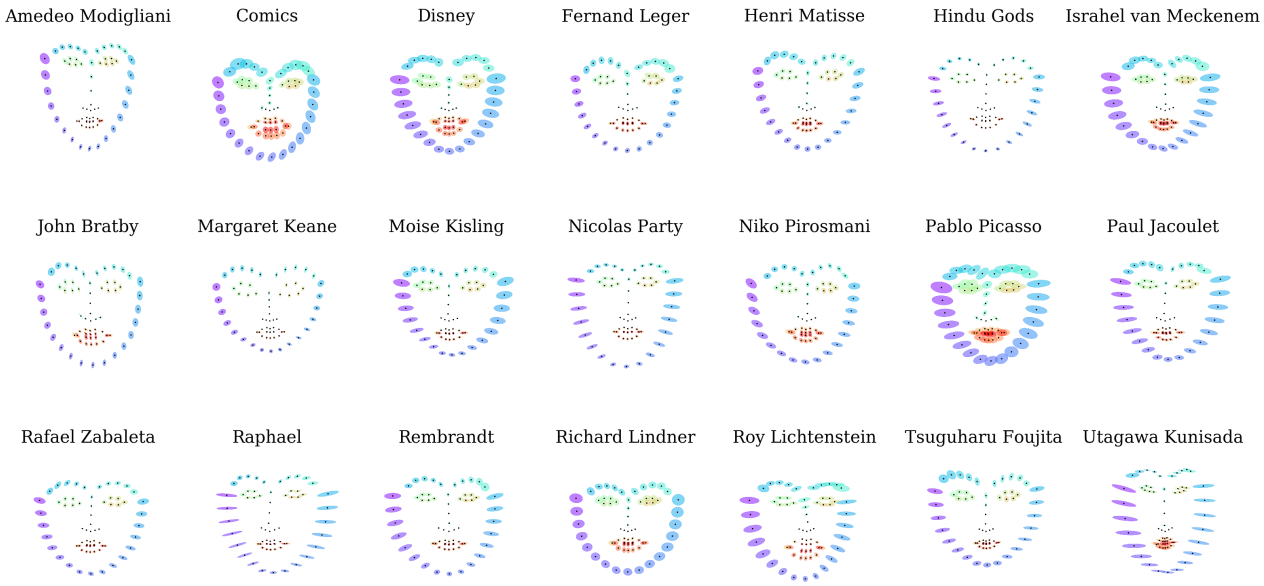

Fig. 5. Various artist distributions using our proposed method for landmark detection in art. Observing artist distributions, we can identify the signature style of each artist. This kind of perceptual analysis can help understanding portrait geometric style, and aid in finding similarities and differences between different artists.

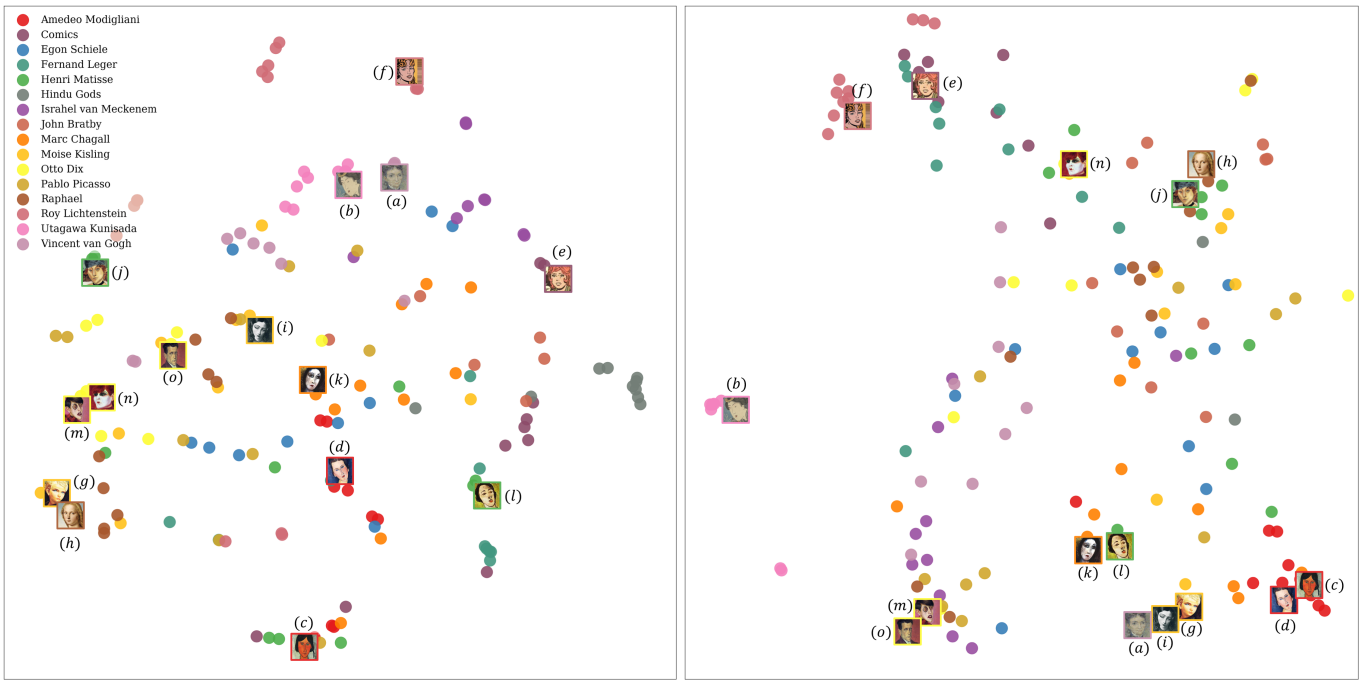

Fig. 6. Comparing style signatures. We show the T-SNE visualization of the Artistic-Faces dataset using Texture style embedding proposed by Gatys et al. (vgg conv_4_3) (left), and our combined texture and geometry signature (right). Notice that by adding geometric information, artworks of artists with consistent geometric style such as Amedeo Modigliani (red points) are clustered closer together at the bottom (on the right). For example, his artworks (c) and (d) are closer together even though they contain different color schemes. On the other hand, artworks of artists with inconsistent geometric style get more scattered on the right embedding space. For example, Otto Dix (yellow points) uses a similar color scheme but has a "caricature-like" geometric style, exaggerating features based on the specific face subject. This geometric style is inconsistent and varies between his artworks and therefore, is more scattered on the right. Specific artworks of different artists such as (k) and (l) have different colors schemes but share a similar geometric style and are therefore, closer when using a combined embedding on the right compared to a texture-only embedding on the left. While artworks that have similar color scheme such as (a) and (b) get separated on the right. In general, we can see that artworks such as (m) and (o), (e) and (f), (a) and (i), which share a similar geometric structure are closer on the right, while artworks such as (m) and (n), (a) and (b), and (g) and (h) that share color and texture but have distinctly different geometric style get separated on the right.

Table 7. Comparisons of inter-ocular Normalized Mean Error (%) on the 300W test sets of natural faces (NF). Last two rows are our method.

Method	Common	Challenging	Full
SDM [2013]	5.57	15.40	7.52
ESR [2014]	5.28	17.00	7.58
LBF [2016]	4.95	11.98	6.32
CFSS [2015]	4.73	9.98	5.76
MDM [2016]	4.83	10.14	5.88
TCDCN [2016]	4.80	8.60	5.54
TR-DRN [2017]	4.36	7.56	4.99
RDR [2017]	5.03	8.95	5.80
PIFA-S [2017]	5.43	9.88	6.30
SAN [2018]	3.41	7.55	4.24
DAN [2017]	3.19	5.24	3.59
DAN-MENPO [2017]	**3.09**	**4.88**	**3.44**
ECT [2018]	4.66	7.96	5.31
$\mathbf{EC_pT_p}$ + **A** (ocular)	3.29	6.34	3.89
$\mathbf{EC_pT_p}$ + **A** (pupil)	4.56	9.16	5.46

X. Xiong and F. De la Torre. 2013. Supervised Descent Method and its Applications to Face Alignment. In *Proceedings of the IEEE Conference on Computer Vision and Pattern Recognition (CVPR)*. 532–539.

H. Zhang, Q. Li, Z. Sun, and Y. Liu. 2018. Combining Data-driven and Model-driven Methods for Robust Facial Landmark Detection. *IEEE Transactions on Information Forensics and Security* 13, 10 (2018), 2409–2422.

Zhanpeng Zhang, Ping Luo, Chen Change Loy, and Xiaoou Tang. 2016. Learning Deep Representation for Face Alignment with Auxiliary Attributes. *IEEE Transactions on Pattern Analysis and Machine Intelligence* 38 (2016), 918–930.

S. Zhu, C. Li, C. Change Loy, and X. Tang. 2015. Face Alignment by Coarse-to-Fine Shape Searching. In *Proceedings of the IEEE Conference on Computer Vision and Pattern Recognition (CVPR)*. 4998–5006.

Fig. 7. Artistic-Faces Dataset samples - part A. From top to bottom: Amedeo Modigliani, Egon Schiele, Henri Matisse and Israhel van Meckenem. Additional samples in Figure 8.

From top-left to bottom-right: Portrait of Leopold Zborowski, 1917 by Amedeo Modigliani courtesy WikiArt [Public Domain] via (https://www.wikiart.org/en/amedeo-modigliani/portrait-of-leopold-zborowski-1917), Portrait of Jeanne Hebuterne, 1918 by Amedeo Modigliani courtesy WikiArt [Public Domain] via (https://www.wikiart.org/en/amedeo-modigliani/portrait-of-jeanne-hebuterne-1918-3), A girl in yellow dress, 1917 by Amedeo Modigliani courtesy WikiArt [Public Domain] via (https://www.wikiart.org/en/amedeo-modigliani/a-girl-in-yellow-dress-1917), Madame Georges van Muyden, 1917 by Amedeo Modigliani courtesy WikiArt [Public Domain] via (https://www.wikiart.org/en/amedeo-modigliani/madame-georges-van-muyd en-1917), Portrait of Pinchus Kremenge, 1916 by Amedeo Modigliani courtesy WikiArt [Public Domain] via (https://www.wikiart.org/en/amedeo-modigliani/portrait-of-pinchus-kremenge-1916), Man with a Glass of Wine, c.1918 by Amedeo Modigliani courtesy WikiArt [Public Domain] via (https://www.wikiart.org/en/amedeo-modigliani/man-with-a-glass-of-wine), Jeanne Hebuterne with Hat and Necklace, 1917 by Amedeo Modigliani courtesy WikiArt [Public Domain] via (https://www.wikiart.org/en/amedeo-modigliani/jeanne-hebuterne-with-hat-and-necklace-1917), Gypsy Woman with a Baby, 1919 by Amedeo Modigliani courtesy WikiArt [Public Domain] via (https://www.wikiart.org/en/amedeo-modigliani/gypsy-woman-with-a-baby-1919),Portrait of Jeanne Hebuterne, 1919 by Amedeo Modigliani courtesy WikiArt [Public Domain] via (https://www.wikiart.org/en/amedeo-modigliani/portrait-of-jeanne-hebuterne-1919-1), Girl with a polka-dot blouse, 1919 by Amedeo Modigliani courtesy WikiArt [Public Domain] via (https://www.wikiart.org/en/amedeo-modigliani/girl-with-a-polka-dot-blouse-1919), Portrait of a Woman with Blue and Green Scarf, 1914 by Egon Schiele courtesy WikiArt [Public Domain] via (https://www.wikiart.org/en/egon-schiele/portrait-of-a-woman-with-blue-and-green-scarf-1914), The Family, 1918 by Egon Schiele courtesy WikiArt [Public Domain] via (https://www.wikiart.org/en/egon-schiele/the-family-1918),Portrait of Valerie Neuzil, 1912 by Egon Schiele courtesy WikiArt [Public Domain] via (https://www.wikiart.org/en/egon-schiele/portrait-of-valerie-neuzil-1912), Portrait of Eduard Kosmack, Frontal, with Clasped Hands, 1910 by Egon Schiele courtesy WikiArt [Public Domain] via (https://www.wikiart.org/en/egon-schiele/portrait-of-eduard-kosmack-frontal-with-clasped-hands-1910), Young Boy, 1918 by Egon Schiele courtesy WikiArt [Public Domain] via (https://www.wikiart.org/en/egon-schiele/young-boy-1918), Head of Dr. Fritsch, 1917 by Egon Schiele courtesy WikiArt [Public Domain] via (https://www.wikiart.org/en/egon-schiele/head-of-dr-fritsch-1917), Russian Prisoner of War with Fur Hat, 1915 by Egon Schiele courtesy WikiArt [Public Domain] via (https://www.wikiart.org/en/egon-schiele/russian-prisoner-of-war-with-fur-hat-1915), Moa, 1911 by Egon Schiele courtesy WikiArt [Public Domain] via (https://www.wikiart.org/en/egon-schiele/moa-1911), Girl in Black Pinafore, Wrapped in Plaid blanket, 1910 by Egon Schiele courtesy WikiArt [Public Domain] via (https://www.wikiart.org/en/egon-schiele/girl-in-black-pinafore-wrapped-in-plaid-blanket-1910), Woman in a Green Blouse and Muff, 1915 by Egon Schiele courtesy WikiArt [Public Domain] via (https://www.wikiart.org/en/egon-schiele/woman-in-a-green-blouse-and-muff-1915), Portrait of Madame Matisse (Green Stripe), 1905 by Henri Matisse courtesy WikiArt [Public Domain US] via (https://www.wikiart.org/en/henri-matisse/portrait-of-madame-matisse-green-stripe-1905), Small Odalisque in Purple Robe, 1937 by Henri Matisse courtesy WikiArt [Fair Use] via (https://www.wikiart.org/en/henri-matisse/small-odalisque-in-purple-robe-1937), The Red Madras Headdress, 1907 by Henri Matisse courtesy WikiArt [Public Domain US] via (https://www.wikiart.org/en/henri-matisse/the-red-madras-headdress-1907), The Ostrich Feather Hat, 1918 by Henri Matisse courtesy WikiArt [Public Domain US] via (https://www.wikiart.org/en/henri-matisse/the-ostrich-feather-hat), Head of Lorette with Curls, 1917 by Henri Matisse courtesy WikiArt [Public Domain US] via (https://www.wikiart.org/en/henri-matisse/head-of-lorette-with-curls-1917), not identified by Henri Matisse courtesy WikiArt [Fair Use] via (https://www.wikiart.org/en/henri-matisse/not-identified-20), Seated Figure, Striped Carpet, 1920 by Henri Matisse courtesy WikiArt [Public Domain US] via (https://www.wikiart.org/en/henri-matisse/seated-figure-striped-carpet-1920), The Ballet Dancer, Harmony in Grey, 1927 by Henri Matisse courtesy WikiArt [Fair Use] via (https://www.wikiart.org/en/henri-matisse/the-ballet-dancer-harmony-in-grey-1927), Purple Robe and Anemones, 1937 by Henri Matisse courtesy WikiArt [Fair Use] via (https://www.wikiart.org/en/henri-matisse/purple-robe-and-anemones-1937), Girl with A Black Cat, 1910 by Henri Matisse courtesy WikiArt [Public Domain US] via (https://www.wikiart.org/en/henri-matisse/girl-with-a-black-cat), Designs for Goldsmiths, 1450-67 by Israhel van Meckenem courtesy The Met Collection [Public Domain] via (https://www.metmuseum.org/art/collection/search/384301), The Knight and the Lady by Israhel van Meckenem-Anonymous courtesy The Met Collection [Public Domain] via (https://www.metmuseum.org/art/collection/search/641804), The Coronation of the Virgin, from The Life of the Virgin by Israhel van Meckenem courtesy The Met Collection [Public Domain] via (https://www.metmuseum.org/art/collection/search/636652), St. James the Greater and St. John, from The Apostles by Israhel van Meckenem courtesy The Met Collection [Public Domain] via (https://www.metmuseum.org/art/collection/search/636599), Saint Elizabeth of Thuringia, c. 1475/1480 by Israhel van Meckenem courtesy NGA Images [Public Domain] via (https://www.nga.gov/collection/art-object-page.3358.html), Saint Stephen by Israhel van Meckenem courtesy NGA Images [Public Domain] via (https://www.nga.gov/collection/art-object-page.3357.html), Saint Ursula and Her Maidens, c. 1475/1480 by Israhel van Meckenem courtesy NGA Images [Public Domain] via (https://www.nga.gov/collection/art-object-page.3362.html), Lute Player and the Harpist, c. 1495/1503 by Israhel van Meckenem courtesy NGA Images [Public Domain] via (https://www.nga.gov/collection/art-object-page.41996.html), Saint Judas Thaddeus, c. 1470/1480 by Israhel van Meckenem courtesy NGA Images [Public Domain] via (https://www.nga.gov/collection/art-object-page.3339.html), Double Portrait of Israhel van Meckenem and His Wife Ida, c. 1490 by Israhel van Meckenem courtesy NGA Images [Public Domain] via (https://www.nga.gov/collection/art-object-page.3311.html).

Fig. 8. Artistic-Faces Dataset samples - part B. From top to bottom: Raphael, Roy Lichtenstein, Utagawa Kunisada, Vincent van Gogh. The dataset also contains Comics and Hindu portraits, as well as artworks by Fernand Leger, John Bratby, Marc Chagall, Moise Kisling, Otto Dix and Pablo Picasso.

From top-left to bottom-right: Portrait of a Man, 1503 by Raphael courtesy WikiArt [Public Domain] via (https://www.wikiart.org/en/raphael/portrait-of-a-man), Portrait of the Young Pietro Bembo, 1504 by Raphael courtesy WikiArt [Public Domain] via (https://www.wikiart.org/en/raphael/portrait-of-the-young-pietro-bembo-1504), Portrait of a Man holding an Apple, 1500 by Raphael courtesy WikiArt [Public Domain] via (https://www.wikiart.org/en/raphael/portrait-of-a-man-holding-an-apple-1500), Portrait of Bindo Altoviti, 1515 by Raphael courtesy WikiArt [Public Domain] via (https://www.wikiart.org/en/raphael/portrait-of-bindo-altoviti-1515), The Pregnant Woman, La Donna Gravida, 1507 by Raphael courtesy WikiArt [Public Domain] via (https://www.wikiart.org/en/raphael/the-pregnant-woman-la-donna-gravida-1507), Joanna of Aragon, 1518 by Raphael courtesy WikiArt [Public Domain] via (https://www.wikiart.org/en/raphael/joanna-of-aragon-1518), Portrait of Cardinal Dovizzi de Bibbiena, 1516 by Raphael courtesy WikiArt [Public Domain] via (https://www.wikiart.org/en/raphael/portrait-of-cardinal-dovizzi-de-bibbiena), Tommaso Fedra Inghrami, 1516 by Raphael courtesy WikiArt [Public Domain] via (https://www.wikiart.org/en/raphael/tommaso-fedra-inghrami), Portrait of a Young Man, 1515 by Raphael courtesy WikiArt [Public Domain] via (https://www.wikiart.org/en/raphael/portrait-of-a-young-man-1515), Portrait of a Lady with a Unicorn, 1506 by Raphael courtesy WikiArt [Public Domain] via (https://www.wikiart.org/en/raphael/portrait-of-a-lady-with-a-unicorn-1506), Girl With Ball, 1961©Estate of Roy Lichtenstein courtesy Image-Duplicator [Fair Use] via (https://www.imageduplicator.com/main.php?decade=60&year=61&work_id=1190), Head Red and Yellow, 1962©Estate of Roy Lichtenstein courtesy Image-Duplicator [Fair Use] via (https://www.imageduplicator.com/main.php?decade=60&year=62&work_id=104#), Little Aloha, 1962 ©Estate of Roy Lichtenstein courtesy Image-Duplicator [Fair Use] via (https://www.imageduplicator.com/main.php?decade=60&year=62&work_id=86), Woman with Peanuts, 1962 ©Estate of Roy Lichtenstein courtesy Image-Duplicator [Fair Use] via (https://www.imageduplicator.com/main.php?decade=60&year=62&work_id=725), Girl in Bath, 1963 ©Estate of Roy Lichtenstein courtesy Image-Duplicator [Fair Use] via (https://www.imageduplicator.com/main.php?decade=60&year=63&work_id=129), Anxious Girl, 1964©Estate of Roy Lichtenstein courtesy Image-Duplicator [Fair Use] via (https://www.imageduplicator.com/main.php?decade=60&year=64&work_id=216), New York World's Fair Mural (Girl in Window), 1964©Estate of Roy Lichtenstein courtesy Image-Duplicator [Fair Use] via (https://www.imageduplicator.com/main.php?decade=60&year=64&work_id=1331), Nurse, 1964©Estate of Roy Lichtenstein courtesy Image-Duplicator [Fair Use] via (https://www.imageduplicator.com/main.php?decade=60&year=64&work_id=219), Vicki! I–I Thought I Heard Your Voice!, 1964©Estate of Roy Lichtenstein courtesy Image-Duplicator [Fair Use] via (https://www.imageduplicator.com/main.php?decade=60&year=64&work_id=248), Reverie, 1965 ©Estate of Roy Lichtenstein courtesy Image-Duplicator [Fair Use] via (https://www.imageduplicator.com/main.php?decade=60&year=65&work_id=3538), Actor and Woman on a Riverbank, 1820-1830 by Utagawa Kunisada courtesy Van Gogh Museum [Public Domain] via (https://www.vangoghmuseum.nl/en/japanese-prints/collection/n0140V1962), Paradise of the First Performance (Kaomise): The Actors Bando Mitsugoro as Hotsuke Chobei and Ichikawa Monnosuke as Hirai Gonpachi, 1831 by Utagawa Kunisada courtesy Van Gogh Museum [Public Domain] via (https://www.vangoghmuseum.nl/en/japanese-prints/collection/n0141V1962), The Actor Iwai Kumesaburo in the Role of the Young Girl Fujikawa of the Ishii Family, 1820-1829 by Utagawa Kunisada courtesy Van Gogh Museum [Public Domain] via (https://www.vangoghmuseum.nl/en/japanese-prints/collection/n0163V1962), Visiting, from the series Fashionable Parody of the Seven Komachi, 1840-1842 by Utagawa Kunisada courtesy Van Gogh Museum [Public Domain] via (https://www.vangoghmuseum.nl/en/japanese-prints/collection/n0170V1962), Edo, from the series Famous Unusual Women from Different Places, 1830-1839 by Utagawa Kunisada courtesy Van Gogh Museum [Public Domain] via (https://www.vangoghmuseum.nl/en/japanese-prints/collection/n0173V1962), Portrait of Sawamura Tosho in the Role of Karukaya Doshin, 1834 by Utagawa Kunisada courtesy Van Gogh Museum [Public Domain] via (https://www.vangoghmuseum.nl/en/japanese-prints/collection/n0175V1962), Two Women with Rice Cakes and Swords, 1844-1845 by Utagawa Kunisada courtesy Van Gogh Museum [Public Domain] via (https://www.vangoghmuseum.nl/en/japanese-prints/collection/n0184V1962), Three Beauties, right sheet of a triptych, 1844-1845 by Utagawa Kunisada courtesy Van Gogh Museum [Public Domain] via (https://www.vangoghmuseum.nl/en/japanese-prints/collection/n0192V1962), An Actor as a Lantern Seller, from the series Six Choices of Summer Among the Night Trades, 1849-1851 by Utagawa Kunisada courtesy Van Gogh Museum [Public Domain] via (https://www.vangoghmuseum.nl/en/japanese-prints/collection/n0195V1962), Special Exhibition of Buddhist Icons at the Tenmangu Shrine, 1849-1851 by Utagawa Kunisada courtesy Van Gogh Museum [Public Domain] via (https://www.vangoghmuseum.nl/en/japanese-prints/collection/n0197V1962), Portrait of a Young Peasant, 1889 by Vincent van Gogh courtesy WikiArt [Public Domain] via (https://www.wikiart.org/en/vincent-van-gogh/portrait-of-a-young-peasant-1889), Self-Portrait, 1889 by Vincent van Gogh courtesy NGA Images [Public Domain] via (https://www.nga.gov/collection/art-object-page.106382.html), La Mousme seduta, 1888 by Vincent van Gogh courtesy NGA Images [Public Domain] via (https://www.nga.gov/collection/art-object-page.46626.html), Head of a Prostitute, 1885 by Vincent van Gogh courtesy Van Gogh Museum [Public Domain] via (https://www.vangoghmuseum.nl/en/collection/s0059V1962), The Zouave, 1888 by Vincent van Gogh courtesy Van Gogh Museum [Public Domain] via (https://www.vangoghmuseum.nl/en/collection/s0067V1962), Head of a Man, 1884-1885 by Vincent van Gogh courtesy Van Gogh Museum [Public Domain] via (https://www.vangoghmuseum.nl/en/collection/s0069V1962), Self-Portrait, 1887 by Vincent van Gogh courtesy Van Gogh Museum [Public Domain] via (https://www.vangoghmuseum.nl/en/collection/s0135V1962v), Self-Portrait, 1887 by Vincent van Gogh courtesy Van Gogh Museum [Public Domain] via (https://www.vangoghmuseum.nl/en/collection/s0155V1962), Portrait of Leonie Rose Charbuy-Davy, 1887 by Vincent van Gogh courtesy Van Gogh Museum [Public Domain] via (https://www.vangoghmuseum.nl/en/collection/s0165V1962), Portrait of Marcelle Roulin, 1888 by Vincent van Gogh courtesy Van Gogh Museum [Public Domain] via (https://www.vangoghmuseum.nl/en/collection/s0167V1962).

Table 8. Geometric Style Signature: Facial Golden Ratios

numerator	denominator	description
$x_{\overline{l\_eye}} - x_{\overline{r\_eye}}$	$x_{42} - x_{39}$	Inter-pupil distance to inner eye corners distance
$x_{54} - x_{48}$	$x_{42} - x_{39}$	mouth width to inner eye corners distance
$y_{\overline{mouth}} - y_8$	$x_{35} - x_{31}$	mouth-chin distance to nose width
$x_{42} - x_{39}$	$y_{57} - y_{51}$	inner eye corners distance to mouth length
$x_{35} - x_{31}$	$x_{39} - x_{36}$	nose width to left eye width
$x_{35} - x_{31}$	$x_{45} - x_{42}$	nose width to right eye width
$x_{35} - x_{31}$	$y_{57} - y_{51}$	nose width to mouth length
$y_{\overline{mouth}} - y_8$	$x_{42} - x_{39}$	mouth-chin distance to inner eye corners distance
$x_{39} - x_{36}$	$y_{\overline{mouth}} - y_{33}$	left eye width to nose-mouth distance
$x_{45} - x_{42}$	$y_{\overline{mouth}} - y_{33}$	right eye width to nose-mouth distance
$y_{57} - y_{51}$	$y_{\overline{mouth}} - y_{33}$	mouth length to nose-mouth distance
$y_{33} - y_8$	$y_{\overline{mouth}} - y_8$	lower face length to mouth-chin distance
$x_{35} - x_{31}$	$y_{\overline{mouth}} - y_{33}$	nose width to nose-mouth distance

Note: x_i refers to the x coordinate of the i^{th} landmark, as defined in [Sagonas et al. 2013], $y_{\overline{f}}$ refers to the y coordinate of the mean point of facial feature f. Facial Golden Ratios obtained from [Schmid et al. 2008].

Table 9. Geometric Style Signature: Neoclassical Canons Facial Ratios

numerator	denominator	description
$x_{54} - x_{35}$	$x_{48} - x_{31}$	mouth width to nose width
$x_{35} - x_{13}$	$x_{31} - x_3$	nose width to face width
$y_{33} - y_{33}$	$y_{27} - y_8$	nose length to lower face length
$x_{42} - x_{35}$	$x_{39} - x_{31}$	inner eye corners distance to nose width
$x_{42} - x_{39}$	$x_{39} - x_{36}$	inner eye corners distance to left eye width
$x_{42} - x_{45}$	$x_{39} - x_{42}$	inner eye corners distance to right eye width

Note: x_i refers to the x coordinate of the i^{th} landmark, as defined in [Sagonas et al. 2013]. Neoclassical Canons facial ratios obtained from [Farkas et al. 1985].